ADVANCED ENERGY MATERIALS
www.advenergymat.de

Nanoflake-Assembled Hierarchical $Na_3V_2(PO_4)_3$/C Microflowers: Superior Li Storage Performance and Insertion/Extraction Mechanism

Qinyou An, Fangyu Xiong, Qiulong Wei, Jinzhi Sheng, Liang He, Dongling Ma, Yan Yao, and Liqiang Mai**

$Na_3V_2(PO_4)_3$ (NVP) has excellent electrochemical stability and fast ion diffusion coefficient due to the 3D Na^+ ion superionic conductor framework, which make it an attractive cathode material for lithium ion batteries (LIBs). However, the electrochemical performance of NVP needs to be further improved for applications in electric vehicles and hybrid electric vehicles. Here, nanoflake-assembled hierarchical NVP/C microflowers are synthesized using a facile method. The structure of as-synthesized materials enhances the electrochemical performance by improving the electron conductivity, increasing electrode–electrolyte contact area, and shortening the diffusion distance. The as-synthesized material exhibits a high capacity (230 mAh g^{-1}), excellent cycling stability (83.6% of the initial capacity is retained after 5000 cycles), and remarkable rate performance (91 C) in hybrid LIBs. Meanwhile, the hybrid LIBs with the structure of NVP || 1 M $LiPF_6$/EC (ethylene carbonate) + DMC (dimethyl carbonate) || NVP and $Li_4Ti_5O_{12}$ || 1 M $LiPF_6$/EC + DMC || NVP are assembled and display capacities of 79 and 73 mAh g^{-1}, respectively. The insertion/extraction mechanism of NVP is systematically investigated, based on in situ X-ray diffraction. The superior electrochemical performance, the design of hybrid LIBs, and the insertion/extraction mechanism investigation will have profound implications for developing safe and stable, high-energy, and high-power LIBs.

1. Introduction

Playing an increasingly important role of energy storage, lithium ion batteries (LIBs) are widely used in portable electronics.[1–4] However, their energy density, power density, and cycling life urgently need to be further improved for applications in electric vehicles and hybrid electric vehicles.[5–8] Achieving breakthroughs in electrode materials is the key to improve the capacity, rate performance, and cycling stability of LIBs.[9–13]

Compared with lithium metal oxides, phosphate cathodes display remarkable electrochemical and thermal stability, which is in favor of the cycling stability.[14,15] Up to now, many phosphate cathode materials, such as $LiFePO_4$,[16,17] $Li_3V_2(PO_4)_3$,[18] $LiVPO_4F$,[19] $Na_3V_2(PO_4)_2F_3$,[20,21] $NaTi_2(PO_4)_3$,[22] and $Na_3V_2(PO_4)_3$ (NVP)[23–25] have been proved to be promising active materials. Among these materials, NVP, a typical Na^+ ion superionic conductor (NASICON)-related compound, exhibits high ion (Li^+, Na^+) mobility due to its open framework with large ion transport tunnels.[26–28] Besides, NVP shows a flat voltage curve with a plateau at ≈3.4 V versus Na^+/Na and has been investigated as one of major prospective cathode materials for sodium ion batteries (SIBs).[23–25] As illustrated in **Scheme 1**a, the smaller ionic radius of Li^+ ion with respect to that of Na^+ ion (0.76 vs 1.06 Å) in principle allows Li^+ ion to diffuse faster in the NVP, which makes NVP more likely to acquire a higher rate performance in LIBs than in SIBs. Recently, NVP as a cathode material for hybrid LIBs has been reported.[27,28] However, rate capability and cycling performance, considered as two important factors which need to be further improved before its widespread applications. In addition, the ion insertion/extraction mechanism of NVP in hybrid LIBs also requires more systematic investigations.

Decreasing the characteristic dimensions of the electrode material is an effective way to improve the rate capability and cycling stability of LIBs.[29–31] In this regard, numerous 2D nanomaterials including $Na_{1.08}V_3O_8$,[5] $Li_4Ti_5O_{12}$ (LTO),[32]

Dr. Q. An, F. Xiong, Q. Wei, J. Sheng, Dr. L. He, Prof. L. Mai
State Key Laboratory of Advanced Technology for Materials Synthesis and Processing
WUT-Harvard Joint Nano Key Laboratory
Wuhan University of Technology
Wuhan 430070, P.R. China
E-mail: mlq518@whut.edu.cn
Dr. Q. An, Dr. Y. Yao
Cullen College of Engineering
Department of Electrical and Computer Engineering
University of Houston
Houston, TX 77204, USA
E-mail: yyao4@central.uh.edu
Prof. D. Ma
Institut National de la Recherche Scientifique (INRS)
1650 Boulevard Lionel-Boulet
Varennes, Quebec, J3X 1S2, Canada

DOI: 10.1002/aenm.201401963

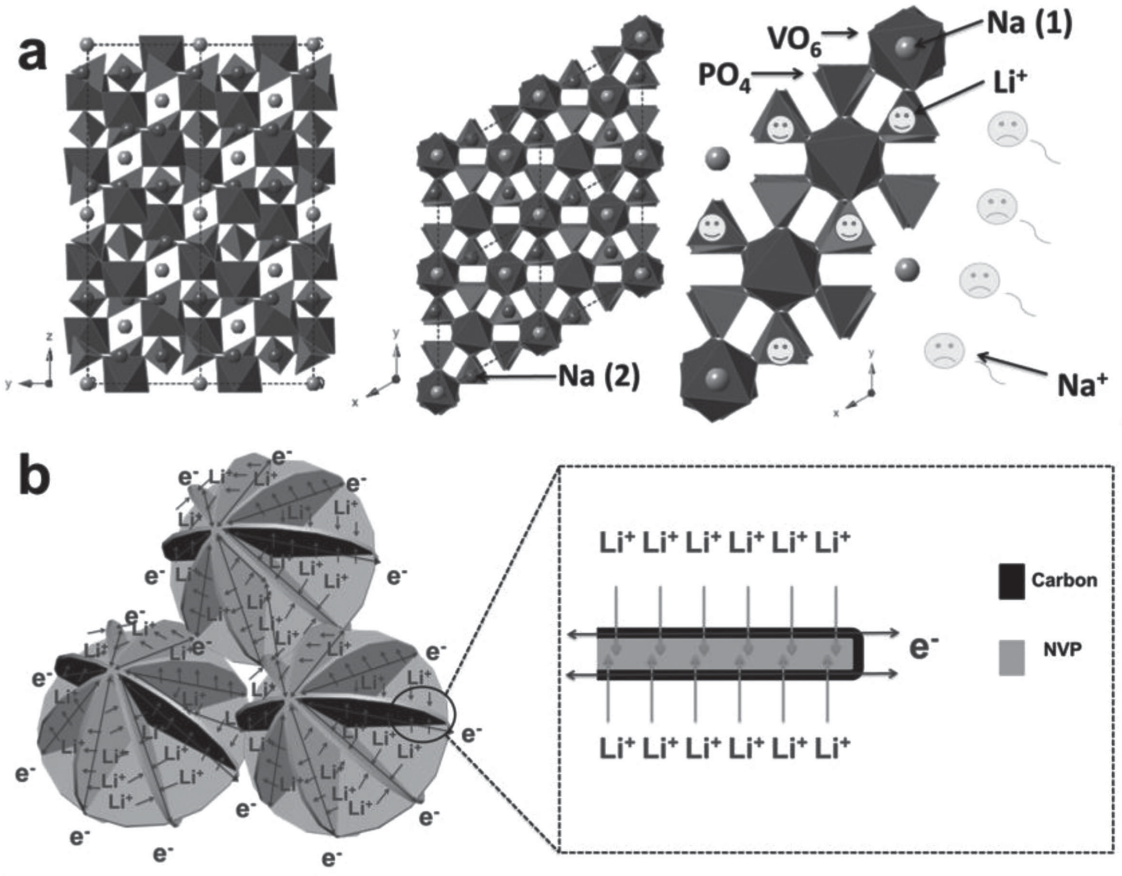

Scheme 1. a) The crystal structure of NVP with a $R\bar{3}c$ space group and the schematic illustration of the comparison for diffusion of Li^+ ion and Na^+ ion in the crystal structure. b) Schematic illustration of electron/ion transport pathways in the nanoflake-assembled hierarchical NVP/C microflowers.

V_2O_5,[33] and TiO_2[7] have recently been synthesized and characterized for improving electrochemical performance of LIBs due to their increased electrode–electrolyte contact area and shortened diffusion distance. However, to obtain an electrode material with excellent cycling stability still remains a big challenge due to the easy agglomeration of 2D nanomaterials caused by their very high surface area and surface energy.[30,34,35] 3D hierarchical nanostructures are believed to have better ability to restrain agglomeration, which is favorable for cycling stability.[34–36] As illustrated in Scheme 1b, nanoflake-assembled hierarchical NVP/C microflowers possess short Li^+ ion diffusion distance and their inter space facilitates the releasing of strain. For the phosphate electrodes, another key problem that needs to be considered is their poor electronic conductivity, which restricts the rate performance and cycling stability.[37–39] Coating NVP with conductive carbon is an effective approach to overcome this problem. The thin uniform coating layer on the nanoflake-assembled microflowers constitutes a 3D electronic transport network, which is favorable to get a high rate performance (Scheme 1b). Therefore, it can be concluded from above analysis that nanoflake-assembled hierarchical NVP/C microflowers hold high promise to greatly improve the electrochemical performance of hybrid LIBs.

Herein, we first report a nanoflake-assembled hierarchical NVP/C microflower electrode material synthesized via a facile precipitation method followed by annealing process. As the electrode for hybrid LIBs, nanoflake-assembled hierarchical NVP/C microflowers exhibit high capacity, excellent rate performance, and cycling stability. Furthermore, their lithium ion insertion/extraction mechanism was systematically investigated by in situ X-ray diffraction (XRD).

2. Results and Discussion

2.1. Morphology and Formation Mechanism Analysis

The morphology of samples was investigated by field emission scanning electron microscopy (FESEM) and transmission electron microscopy (TEM). As shown in **Figure 1**a, the precursor is composed of nanoflake-assembled flower-like microsphere with a size of ≈1–2 μm in diameter and the thickness of constituent nanoflakes is 20–40 nm. Remarkably, the hierarchical flower-like structure is maintained even after high-temperature annealing at 750 °C (NVP-750) and there is no discernible structural collapse or breakage in the sample (Figure 1b,c). In addition, neighboring nanoflakes are loosely interconnected with obvious open spaces existing between them. The TEM images of NVP-750 show conspicuous hierarchical flower-like structures which are composed of nanoflakes (Figures 1d and

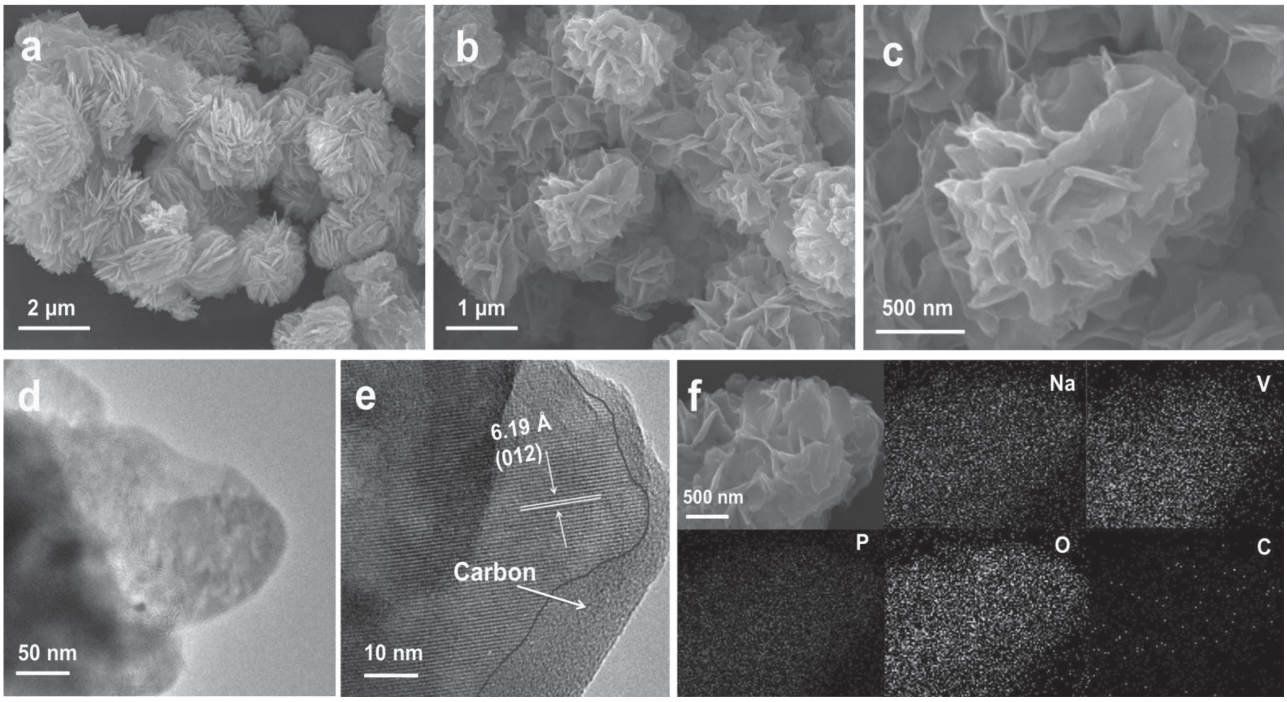

Figure 1. a) FESEM image of precursor. b,c) FESEM images, d,e) TEM images, and f) EDS elemental mapping of nanoflake-assembled hierarchical NVP/C microflowers annealed at 750 °C.

S2, Supporting Information). The FESEM and TEM images of NVP-650 (annealed at 650 °C) display a similar morphology, but with the annealing temperature being further increased to 850 °C (NVP-850), the nanoflakes were fused to form somewhat a bulk structure (Figures S1 and S3, Supporting Information). The FESEM image of precursor without glucose (Figure S1c, Supporting Information) shows similar hierarchical flower-like morphology, indicating that the effect of glucose on the morphology during the forming of precursor can be ignored. However, the morphology of the precursor without glucose has been destroyed after annealing, implying that the existence of glucose is in favor of the morphology maintenance (Figure S1d, Supporting Information). This can be attributed to the carbon layer forming from the carbonization of glucose during the preheating, which is effective to restrain the agglomeration. The high resolution TEM (HRTEM) image clearly shows the lattice fringes with the space of 6.19 Å, corresponding to the *d*-spacing of the (012) planes of rhombohedral NVP, indicating the crystalline nature of the nanoflakes in the NVP-750 sample (Figure 1e). The carbon layer with a thickness of 5–10 nm can also be observed. In addition, energy dispersive spectrometry (EDS) element mappings display that Na, V, P, O, and C are homogeneously distributed in NVP-750 (Figure 1f).

The schematic illustration of the fabrication of nanoflake-assembled NVP/C hierarchical microflowers is shown in **Scheme 2**. The as-synthesized material was obtained through water bath and annealing treatment, while the microflower morphology was generated during the water bath. In order to investigate the formation process of nanoflake-assembled microflowers, a series of time dependent experiments were carried out. The FESEM images (Figure S4, Supporting Information) reveal that a solid structure is formed immediately after the addition of *n*-propanol and then gradually grows to form flower-like microparticles at ≈10 min. The possible formation mechanism is that the *n*-propanol decreases the polarity of solvent and the solubility of solutes, so called antisolvent crystallization[40,41] (the water as solvent and the *n*-propanol as antisolvent), leading to the nucleation. The morphology evolution from irregular particles to nanoflake-assembled microflowers may be due to the Ostwald ripening process, although the exact mechanism is currently under further investigation.

2.2. Structure Characterization

The phase purity and crystallinity of the NVP-750 were characterized by XRD (**Figure 2**a). All the diffraction peaks can be readily indexed to the NASICON structured NVP with a $R\bar{3}c$ space group (rhombohedral unit cell), corresponding well to the previously reported literatures.[37,42,43] No other phases can be detected, which confirms the high phase purity of NVP-750. Moreover, the result of inductively coupled plasma (ICP) analysis shows that the molar ratio of Na, V, and P is 1.53:1.00:1.48 in the NVP-750, further confirming the phase. The intensity of NVP-650 is lower than NVP-750 (Figure S5b, Supporting Information). Besides, the full width at half maximum (FWHM) of the several main XRD peaks of NVP-650 is larger than that of NVP-750 (Table S1, Supporting Information). These results indicate that the crystallinity of NVP-650 is lower than that of NVP-750. Some obvious peaks of impurity are observed in the XRD pattern of NVP-850 (Figure S5c, Supporting Information) due to overhigh annealing temperature.[37] The Raman spectrum of NVP-750 (Figure 2b) displays two characteristic bands of carbonaceous materials located

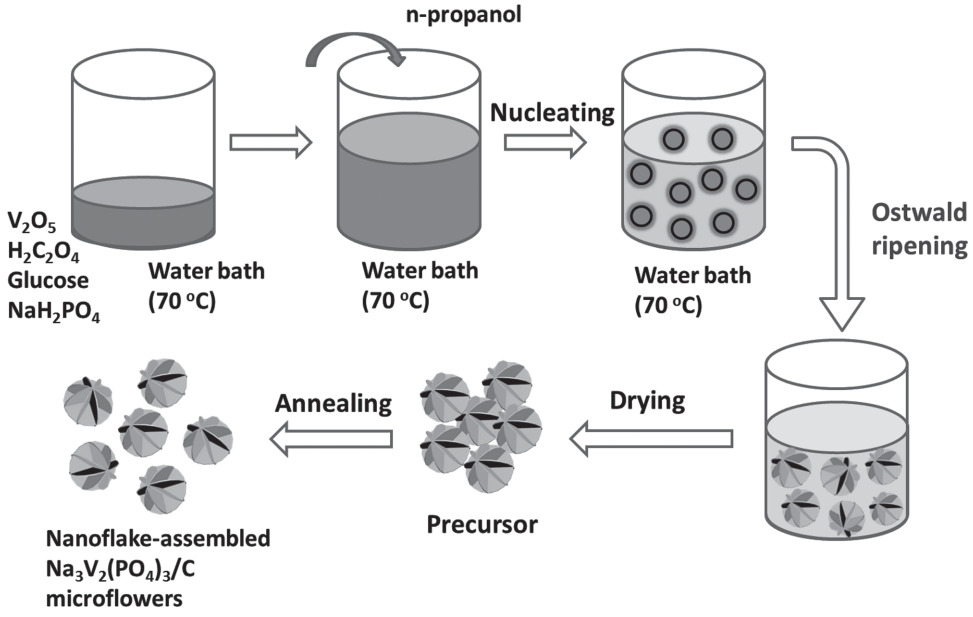

Scheme 2. Schematic illustration of the fabrication of nanoflake-assembled NVP/C hierarchical microflowers.

at 1339 cm^{-1} (D-band, disorder-induced phonon mode) and 1593 cm^{-1} (graphite G-band), respectively, indicating that the deposited carbon is partially graphitized.[43,44] The Raman spectrum of the sample without adding any glucose and annealed at 750 °C (Figure S6, Supporting Information) displays the similar result, which may be attributed to the carbonization of $C_2O_4^{2-}$ anions during annealing. In addition, the carbon contents of NVP-650, NVP-750, NVP-850, and the sample without adding glucose annealing at 750 °C are 5.2%, 4.8%, 2.9%, and 0.1%, respectively, based on the elemental analysis of C, H, and N. It strongly suggests the importance of glucose during the sample synthesis for carbon coating. The pore structure

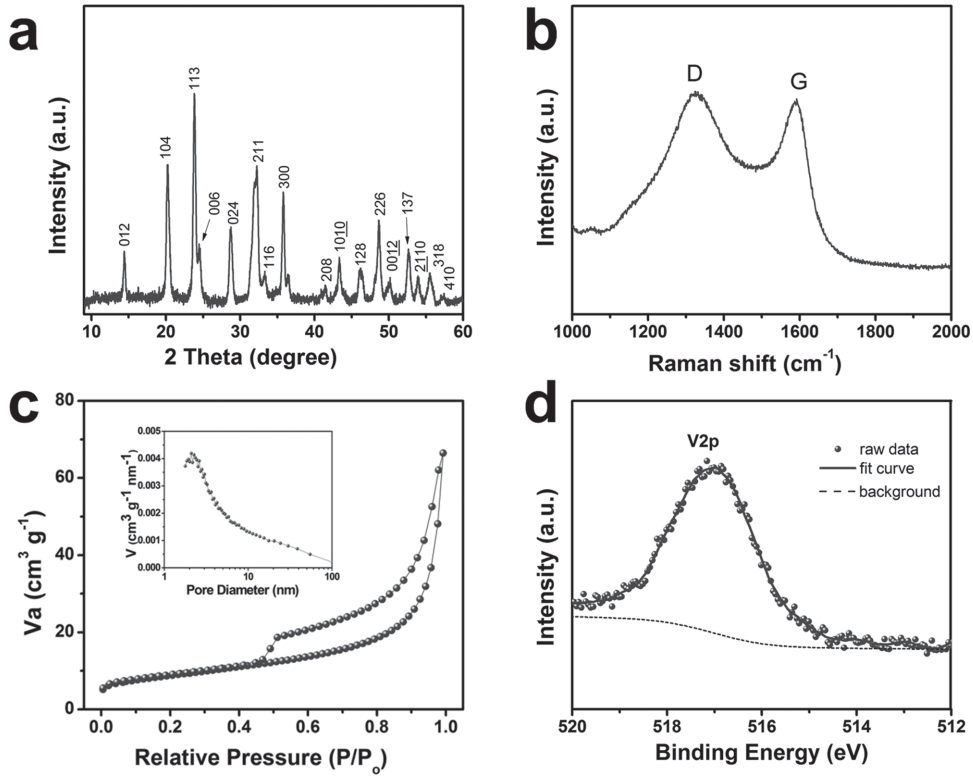

Figure 2. Structural characterization of NVP-750: a) XRD pattern, b) Raman spectrum, c) nitrogen adsorption–desorption isotherm and corresponding pore size distribution (inset), and d) XPS pattern.

and surface area of NVP-750 were investigated by nitrogen isothermal–adsorption technique (Figure 2c). The isotherm can be described as type II with a H3 hysteresis loop. The Brurauer–Emmerr–Teller (BET) surface area of NVP-750 is estimated to be 30.7 $m^2 g^{-1}$, which is much larger than that of NVP-850 (12.8 $m^2 g^{-1}$) (Figure S7, Supporting Information). This result indicates that when annealing temperature is too high, sample agglomeration occurs, which results in the decrease of BET surface. The Barret–Joyner–Halenda pore-size distribution curve (inset of Figure 2c) displays that the pore sizes in NVP-750 are mainly below 20 nm. The X-ray photoelectron spectrum (XPS) (Figure 2d) was utilized to probe the oxidation state of vanadium in NVP-750. A peak located at the binding energy of 517.01 eV, corresponding to V^{3+}, was observed.[44–47]

2.3. Electrochemical Performance

In order to investigate the electrochemical performance of NVP, the coin cells with metallic lithium as anode were assembled. First, NVP electrodes were measured in a wide voltage window between 1.0 and 4.3 V versus Li^+/Li to obtain high capacity. The reversible capacity of carbon in the composite is negligible due to the fact that the discharge voltage of carbonaceous materials is below 1.0 V.[48] Cyclic voltammetry (CV) curves (**Figure 3**a) show two pairs of oxidation and reduction peaks, at about 3.90/3.60 and 1.83/1.66 V, which are close to the equilibrium voltages of V^{4+}/V^{3+} and V^{3+}/V^{2+} in our sample, respectively.[49] Galvanostatic discharge/charge measurements were carried out in order to compare the electrochemical performance of NVP annealed at different temperatures. The results of low current density (0.91 C, 1 C refers to 110 mA g^{-1}) charge/discharge cycles (Figure 3b) show that the initial discharge capacity of NVP-750 is 230 mAh g^{-1}, which is close to the capacity corresponding to 4 Li^+ ion insertion and higher than those of NVP-650 (223 mAh g^{-1}) and NVP-850 (121 mAh g^{-1}), respectively. Note that the cycling stability and reversible capacity of NVP-650 and NVP-750 are very similar during the first 15 cycles, while capacity of NVP-650 drop after 20 cycles. This is attributed to the low crystallinity of NVP-650, which leads to poor stability of crystal, especially during a great quantity of ions (four ions per formula) insertion/extraction resulting in a large expansion.[5,50,51] After 50 cycles, the discharge capacities of NVP-650, NVP-750, and NVP-850 are 105, 209, and 25 mAh g^{-1}, corresponding to 47.1%, 90.9%, and 20.7% of their initial capacities, respectively, indicating that NVP-750 exhibits better long-term performance. And the Coulombic efficiency of NVP-750 is close to 100%. Moreover, two voltage plateaus of NVP-750 are clearly observed from the charge/discharge curves, which are longer than those of other two samples (Figure 3c). Furthermore, the Nyquist plot (Figure S8, Supporting Information) shows that the charge transfer resistance (Rct) of NVP-750 is much lower than those of NVP-650 and NVP-850. This is on account of that the increased annealing temperature can increase the electronic conductivity of carbon and the ionic diffusion coefficient by enhancing the crystallization, but the overhigh temperature annealing leads to agglomeration which is adverse for the electronic conduction and ion diffusion. Besides, the existence of impurity in NVP-850 is another reason for the poor

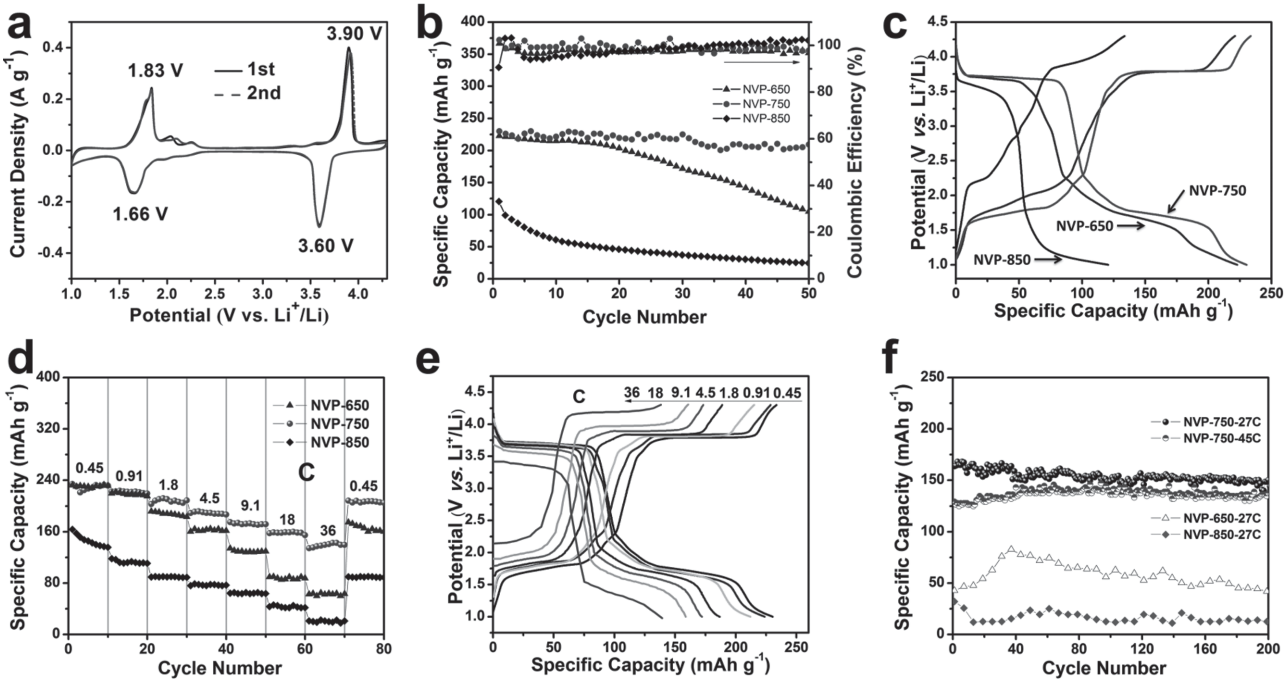

Figure 3. The electrochemical performance of NVP in the potential range from 1.0 to 4.3 V (vs Li^+/Li): a) CV curves of NVP-750 at a scan rate of 0.1 mV s^{-1}; b) cycling performance and c) charge/discharge curves of NVP-650, NVP-750, and NVP-850 at the current density of 0.91 C; d) rate performance of NVP-650, NVP-750, and NVP-850, and e) corresponding charge/discharge curves of NVP-750; f) high-rate cycling performance of NVP-650, NVP-750, and NVP-850.

electrochemical performance. Further, the electrochemical performance of the sample prepared under the same conditions as NVP-750 with the lack of glucose was also investigated (Figure S9, Supporting Information). The result shows a low retention (22.6%) of performance after 50 cycles with low initial capacity (88 mAh g^{-1}). The low initial capacity of the sample with glucose can be attributed to the low carbon content and the agglomeration, which results in poor electronic conductivity and long ion diffusion distance, respectively, indicating that suitable carbon coating is necessary for improving the electrochemical performance. NVP-750 also displays excellent rate performance. A high discharge capacity (143 mAh g^{-1}) of NVP-750 was retained even at 36 C, which is higher than that of NVP-650 (64 mAh g^{-1}) and NVP-850 (23 mAh g^{-1}) (Figure 3d). In addition, the cycling stability of NVP-750 at high current density is shown in Figure 3f. The initial specific discharge capacities are 164 and 130 mAh g^{-1} at the rates of 27 and 45 C, respectively. Remarkably, their capacities are retained at 150 and 138 mAh g^{-1} after 200 cycles, respectively. The initial capacities of NVP-650 (43 mAh g^{-1}) and NVP-850 (32 mAh g^{-1}) at 27 C are lower than that of NVP-750. These above electrochemical analyses confirm the best electrochemical performance of NVP-750 among the three samples.

Furthermore, the electrochemical performance of NVP as a high potential cathode has been investigated at a voltage window between 2.5 and 4.3 V. The CV curves of NVP-750 (**Figure 4**a) show that one couple of oxidation and reduction peaks appear at potential about 3.85/3.66 V, essentially corresponding to those observed in the CV curves measured at 1.0–4.3 V. NVP-750 electrode delivers the initial capacity of 103 mAh g^{-1} and exhibits no evident capacity loss after 50 cycles at the low current density of 0.91 C (Figure 4b). The stable voltage can also be confirmed in the charge/discharge curves (Figure 4c). NVP-750 displays excellent rate performance and a discharge capacity of 43 mAh g^{-1} was still retained even at a high rate of 91 C (Figure 4d). Compared to the reported results, NVP-750 exhibits the better rate performance whether using two plateaus or only the high potential plateau (Figure S10, Supporting Information). The excellent rate performance can be ascribed to the short ionic diffusion distance of nanoflakes and the fast electronic transport network of carbon layer. NVP-750 also exhibits excellent stability at 9.1 C. The initial capacity of 86 mAh g^{-1} has been obtained and 83.6% of it is retained after 5000 cycles (Figure 4e). The cycling stability is much better than the best one has been reported (capacity retention is 97.4% over the following 97 cycles).[27] This can be attributed to the stability of 3D hierarchical structure and the buffering for the stress of Li^+ ion insertion/extraction during charge and discharge cycles provided by the space between nanoflakes.

Meanwhile, the electrochemical performance of NVP-750 as anode for hybrid LIBs has also been investigated by measurements in a voltage window between 1.0 and 2.5 V. The oxidation and reduction peaks (1.83/1.73 V) of V^{3+}/V^{2+} in NVP-750 can be clearly observed from their CV curves (**Figure 5**a). Cycling at a low current of 0.91 C, its initial capacity is 99 mAh g^{-1} and the capacity of 98 mAh g^{-1} can be retained after 50 cycles, corresponding to capacity retention of 99.0% with Coulombic efficiency closing to 100% (Figure 5b). NVP-750 electrode displays excellent rate performance with a discharge capacity of 72 mAh g^{-1} can be obtained even at a high rate of 91 C (Figure 5d). NVP-750 also exhibits excellent stability at 9.1 C. The initial capacity of 77 mAh g^{-1} has been obtained and 97.5% is retained after 7000 cycles (Figure 5e).

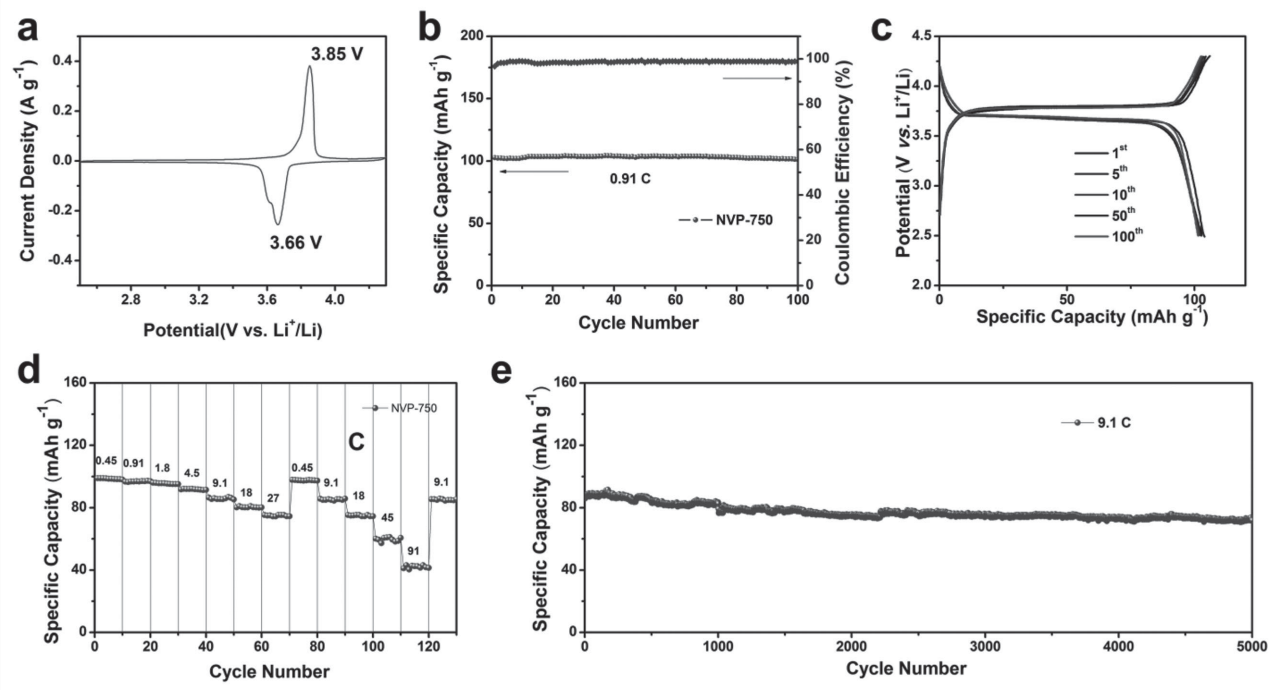

Figure 4. The electrochemical performance of NVP-750 in the potential range from 2.5 to 4.3 V (vs Li^+/Li): a) CV curve at a scan rate of 0.1 mV s^{-1}; b) cycling performance, and c) charge/discharge curves at the current density of 0.91 C; d) rate performance and e) high-rate cycling performance.

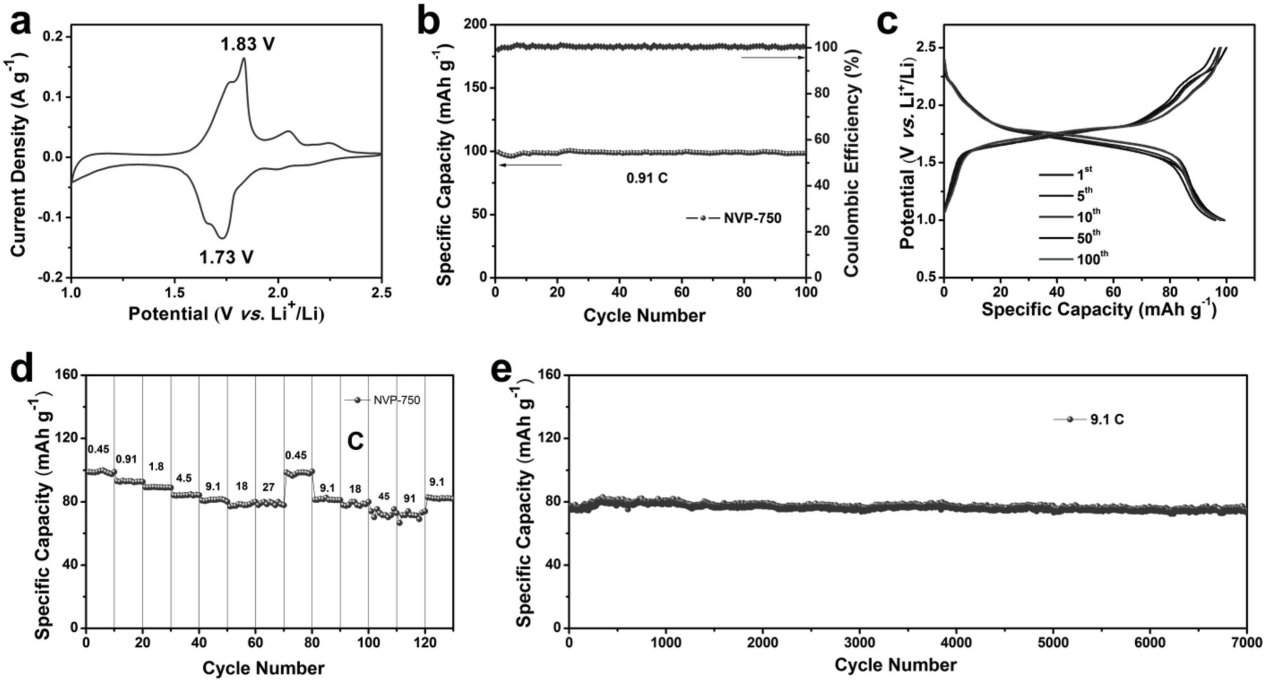

Figure 5. The electrochemical performance of NVP-750 in the potential range from 1.0 to 2.5 V (vs Li^+/Li): a) CV curve at a scan rate of 0.1 mV s^{-1}; b) cycling performance and c) charge/discharge curves at the current density of 0.91 C; d) rate performance and e) high-rate cycling performance of NVP-750.

Taking advantage of the large voltage difference between the two plateaus of NVP, a symmetric hybrid LIB with a structure of NVP ‖ 1 M $LiPF_6$/EC (ethylene carbonate) + DMC (dimethyl carbonate) ‖ NVP (NVP – NVP) was assembled. The scheme of the structure and the mechanism of the symmetric hybrid LIB are shown in **Figure 6**a. In addition, an asymmetric hybrid LIB with structure as LTO ‖ 1 M $LiPF_6$/EC + DMC ‖ NVP (NVP – LTO) was assembled. When measure at 100 mA g^{-1} with a potential range of 1.0–3.0 V, the initial discharge capacity of 79 and 73 mAh g^{-1} can be obtained from NVP – NVP and NVP – LTO, respectively (Figure 6b).

The excellent electrochemical performance of NVP/C microflowers can be ascribed to the advantages of their ionic properties and the favorable structure. (a) The large insertion channels of NASICON structure and the small size of Li^+ ion are beneficial to the ionic transport. (b) The nanostructure possesses the large electrode–electrolyte contact area and short ion diffusion distance, and the space between nanoflakes provides a buffer for the stress associated with Li^+ ion insertion/extraction during charge and discharge. (c) The electronic conduction network established by carbon layer ensures the fast electron transport between NVP nanoflakes.

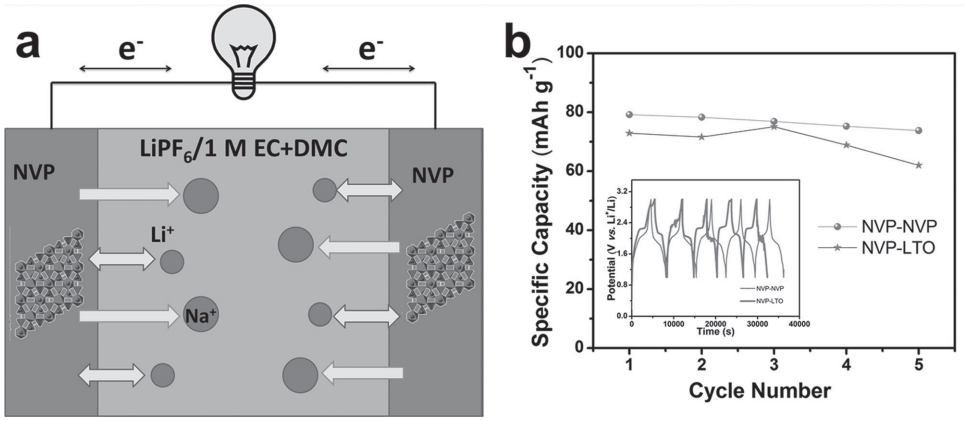

Figure 6. a) Schematic Illustration of the structure and mechanism of the symmetric hybrid LIBs with a structure of NVP ‖ 1 M $LiPF_6$/EC + DMC ‖ NVP (NVP – NVP) and b) the cycling performance and the corresponding potential-times curves (inset) of symmetric hybrid LIBs and asymmetric hybrid LIBs with structure as $Li_4Ti_5O_{12}$ ‖ 1 M $LiPF_6$/EC + DMC ‖ NVP (NVP – LTO) measured at 100 mA g^{-1} in the voltage range of 1–3 V.

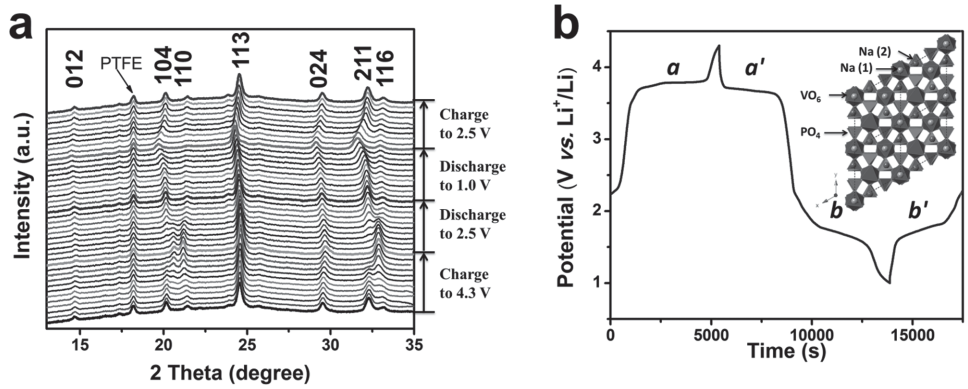

Figure 7. a) In situ XRD patterns of NVP-750/Li cell during the charge/discharge in a voltage range of 1.0–4.3 V and b) corresponding potential-time curves.

2.4. Insertion/Extraction Mechanism

Furthermore, the in situ XRD technique has been utilized to investigate the insertion/extraction mechanism of the NVP as electrode for hybrid LIBs (**Figure 7**a). The 2θ (°) were recorded from 13° to 35°, a range that can well reflect structural changes of NVP as electrode for hybrid LIBs during the first cycle between 1.0 and 4.3 V at a low current. At the beginning of the charging process, all the peaks can be identified as $Li_2NaV_2(PO_4)_3$, corresponding well to the literature previously reported, except for the peaks from binder (poly(tetrafluoroethylene) (PTFE)).[26] This result indicates that ion-exchange takes place between the NVP and 1 M $LiPF_6$/EC + DMC electrolyte during the standing of the assembled cell, which was also supported by the result of ICP analysis. Moreover, the ion-exchange reaction can be confirmed by the XRD pattern of NVP-750 soaked in 1 M $LiPF_6$/EC + DMC electrolyte for 12 h (Figure S11, Supporting Information), where the phase of $Li_2NaV_2(PO_4)_3$, instead of NVP, was undoubtedly observed. With continuous charging, some new peaks of $NaV_2(PO_4)_3$ appear and gradually strengthen while the peaks arising from NVP weaken. This process can be considered as coexistence of two phases, indicating that the reaction at plateau *a* of the corresponding potential-time curves (Figure 7b) is the phase transition from $Li_2NaV_2(PO_4)_3$ to $NaV_2(PO_4)_3$. At the end of charging (4.3 V), the XRD pattern can be indexed to $NaV_2(PO_4)_3$, corresponding well to the previous reported literature.[42] At the beginning of the discharge, the intensities of partial peaks from $NaV_2(PO_4)_3$ decrease with peaks of $Li_2NaV_2(PO_4)_3$ appearing and strengthening. Upon discharging to 2.5 V, all the peaks can be identified as $Li_2NaV_2(PO_4)_3$, confirming the phase completely transforms back to $Li_2NaV_2(PO_4)_3$. With further discharging, several main peaks such as (012), (104), (113), (024), and (211) shift to smaller angles, indicating that the *d*-space increases during the ions insertion. However, no new peaks appear or peaks disappear during this process, indicating the coexistence of two phases does not occur at the plateau *b*. After discharging to 1.0 V, the phase of $Li_4NaV_2(PO_4)_3$ can be concluded from the capacity (230 mAh g^{-1}) which corresponds to 4 Li^+ ion insertion. In addition, after recharging back to 2.5 V, the peaks shift back to their original positions suggesting the reversible phase transformation back to $Li_2NaV_2(PO_4)_3$. Based on the above analysis, the possible Li^+ ion insertion/extraction mechanism of NVP as electrode for hybrid LIBs can be described as follows:

$$\text{(Standing)}\ Na_3V_2(PO_4)_3 + 2Li^+ \rightarrow Li_2NaV_2(PO_4)_3 + 2Na^+ \quad (1)$$

$$\text{(Plateau a)}\ Li_2NaV_2(PO_4)_3 \leftrightarrow NaV_2(PO_4)_3 + 2Li^+ + 2e^- \quad (2)$$

$$\text{(Plateau b)}\ Li_2NaV_2(PO_4)_3 + 2Li^+ + 2e^- \leftrightarrow Li_4NaV_2(PO_4)_3 \quad (3)$$

3. Conclusions

The nanoflake-assembled hierarchical NVP/C (NVP-750) microflowers have been successfully synthesized by a facile method. The NVP-750 exhibits promising properties for hybrid LIBs with high capacity, excellent rate performance, and remarkable cycling stability. A high capacity of 230 mAh g^{-1} can be obtained at 0.91 C in a voltage range from 1.0 to 4.3 V, which is significant for the applications in LIBs with high energy density. As the high potential cathode for hybrid LIBs, the high rate charge/discharge properties are outstanding: i.e., it can be charged/discharged at high rates of 91 C with a capacity of 43 mAh g^{-1}. Besides, 83.6% of the initial capacity can be retained after 5000 cycles at 9.1 C, which is attractive for the development of hybrid LIBs with high power density and long-term cycling stability. Hence, nanoflake-assembled hierarchical NVP/C microflower would be a promising cathode material for safe and stable, high-energy and high-power LIBs. Furthermore, the insertion/extraction mechanism of nanoflake-assembled hierarchical NVP/C microflowers as electrode in hybrid LIBs has been investigated by in situ XRD, which provides invaluable information for tailoring the kinetic barrier to optimize the physical and electrochemical properties of electrode materials.

4. Experimental Section

Synthesis and Physicochemical Characterization: V_2O_5, $H_2C_2O_4{\cdot}2H_2O$, $NaH_2PO_4{\cdot}2H_2O$, and glucose, of analytical grade, were all purchased

from the Sinopharm Chemical Reagent Co., Ltd. (Shanghai, China). For a typical synthesis, V_2O_5 (0.36 g) and $H_2C_2O_4{\cdot}2H_2O$ (0.76 g) were dissolved into deionized water (20 mL) and vigorously stirred at 70 °C for 1 h to obtain a VOC_2O_4 solution. Then $NaH_2PO_4{\cdot}2H_2O$ (0.94 g) and glucose (0.2 g) were added into the solution, which was further stirred for stirring 5 min. After that, *n*-propanol (50 mL) was added into the solution stirring was continued for more than 10 min, followed by drying at 70 °C to get nanoflake-assembled flower-like precursor. In the end, nanoflake-assembled hierarchical NVP/C microflowers were obtained from the precursor by preheating it at 400 °C for 4 h followed by annealing at 750 °C for 8 h in argon atmosphere with a heating rate of 5 °C min^{-1}. A series of experiments with different annealing temperatures and without glucose were carried out in order to identify the optimal synthesis recipe. XRD and in situ XRD measurements were performed to investigate the crystallographic structure using a D8 Advance X-ray diffractometer with a nonmonochromated Cu Kα X-ray source. FESEM images were collected with a JEOL-7100F microscope at an acceleration voltage of 10 kV. TEM and HRTEM images were recorded by using a JEM-2100F STEM/EDS microscope. BET surface areas were measured using a Tristar II 3020 instrument by adsorption of nitrogen at 77 K. XPS measurement was performed using a VG Multi Lab 2000 instrument. The carbon content analyses were performed by Elementar Vario EL cube elemental analyzer. ICP test were performed by PerkinElmer Optima 4300DV spectrometer.

Electrochemical Characterization: The electrochemical properties were characterized by assembling 2016 coin cells in a glove box filled with pure argon gas, which used lithium pellet as the anode. The electrolyte is composed of 1 M $LiPF_6$ dissolved in EC/DMC with a volume ratio of 1:1. Cathode electrodes were obtained with 60% nanoflake-assembled hierarchical NVP/C microflowers, 30% acetylene black and 10% PTFE. Galvanostatic charge/discharge cycling behavior was investigated in a potential range of 1.0–4.3/2.5–4.3/1.0–2.5 V versus Li^+/Li with a multichannel battery testing system (LAND CT2001A). CV and AC-impedance spectra were acquired with an electrochemical workstation (Autolab PGSTAT 302 and CHI 760D).

Supporting Information

Supporting Information is available from the Wiley Online Library or from the author.

Acknowledgements

Q.A. and F.X. contributed equally to this work. All authors discussed the results and commented on the paper. The authors declare no competing financial interest. This work was supported by the National Basic Research Program of China (2013CB934103 and 2012CB933003), the National Natural Science Foundation of China (51272197), the National Science Fund for Distinguished Young Scholars (51425204), the International Science and Technology Cooperation Program of China (2013DFA50840), the Hubei Science Fund for Distinguished Young Scholars (2014CFA035), the Fundamental Research Funds for the Central Universities (WUT:2014-YB-001 and WUT:2014-CL-B1-12), the State Key Laboratory of Advanced Technology for Materials Synthesis and Processing (Wuhan University of Technology) (2013-KF-9, 2014-KF-4 and 2013-ZD-7), and the Students Innovation and Entrepreneurship Training Programs (20141049701006 and 20141049701027). The authors thank Prof. C. M. Lieber of Harvard University, Prof. Dongyuan Zhao of Fudan University, and Dr. Jun Liu of Pacific Northwest National Laboratory for strong support and stimulating discussion.

Received: November 4, 2014
Revised: December 21, 2014
Published online:

[1] J. M. Tarascon, M. Armand, *Nature (London)* **2001**, *414*, 359.
[2] P. G. Bruce, S. A. Freunberger, L. J. Hardwick, J. M. Tarascon, *Nat. Mater.* **2012**, *11*, 19.
[3] N. Recham, J. N. Chotard, L. Dupont, C. Delacourt, W. Walker, M. Armand, J. M. Tarascon, *Nat. Mater.* **2010**, *9*, 68.
[4] K. Kang, Y. S. Meng, J. Bréger, C. P. Grey, G. Ceder, *Science* **2006**, *311*, 977.
[5] H. Y. Wang, S. Q. Liu, Y. Ren, W. J. Wang, A. D. Tang, *Energy Environ. Sci.* **2012**, *5*, 6173.
[6] S. Q. Wang, S. R. Li, Y. Sun, X. Y. Feng, C. H. Chen, *Energy Environ. Sci.* **2011**, *4*, 2854.
[7] S. B. Yang, X. L. Feng, K. Müllen, *Adv. Mater.* **2011**, *23*, 3575.
[8] H. Wu, G. Chan, J. W. Choi, I. Ryu, Y. Yao, M. T. McDowell, S. W. Lee, A. Jackson, Y. Yang, L. B. Hu, Y. Cui, *Nat. Nanotechnol.* **2012**, *7*, 309.
[9] J. Liu, J. G. Zhang, Z. G. Yang, J. P. Lemmon, C. Imhoff, G. L. Graff, L. Y. Li, J. Z. Hu, C. M. Wang, J. Xiao, G. Xia, V. V. Viswanathan, S. Baskaran, V. Sprenkle, X. L. Li, Y. Y. Shao, B. Schwenzer, *Adv. Funct. Mater.* **2013**, *23*, 929.
[10] Y. Yao, M. T. McDowell, I. Ryu, H. Wu, N. Liu, L. B. Hu, W. D. Nix, Y. Cui, *Nano Lett.* **2011**, *11*, 2949.
[11] J. W. Fergus, *J. Power Sources* **2010**, *195*, 939.
[12] D. Chao, X. Xia, J. Liu, Z. Fan, C. F. Ng, J. Lin, H. Zhang, Z. X. Shen, H. J. Fan, *Adv. Mater.* **2014**, *26*, 5794.
[13] C. He, S. Wu, N. Zhao, C. Shi, E. Liu, J. Li, *ACS Nano* **2013**, *7*, 4459.
[14] L. S. Plashnitsa, E. Kobayashi, Y. Noguchi, S. Okada, J. Yamakia, *J. Electrochem. Soc.* **2010**, *157*, A536.
[15] S. B Yang, Y. J. Gong, Z. Liu, L. Zhan, D. P. Hashim, L. L. Ma, R. Vajtai, P. M. Ajayan, *Nano Lett.* **2013**, *13*, 1596.
[16] H. Liu, F. C. Strobridge, O. J. Borkiewicz, K. M. Wiaderek, K. W. Chapman, P. J. Chupas, C. P. Grey, *Science* **2014**, *344*, 1252817.
[17] S. W. Oh, S. T. Myung, S. M. Oh, K. H. Oh, K. Amine, B. Scrosati, Y. K. Sun, *Adv. Mater.* **2010**, *22*, 4842.
[18] Q. Wei, Q. Y. An, D. D. Chen, L. Q. Mai, S. Y. Chen, Y. L. Zhao, K. M. Hercule, L. Xu, A. Minhas-Khan, Q. Z. Zhang, *Nano Lett.* **2014**, *14*, 1042.
[19] J. M. AtebaMba, C. Masquelier, E. Suard, L. Croguennec, *Chem. Mater.* **2012**, *24*, 1223.
[20] R. A. Shakoor, D.-H. Seo, H. Kim, Y.-U. Park, J. Kim, S.-W. Kim, H. Gwon, S. Lee, K. Kang, *J. Mater. Chem.* **2012**, *22*, 20535.
[21] W. Song, S. Liu, *Solid State Sci.* **2013**, *15*, 1.
[22] S. I. Park, I. Gocheva, S. Okada, J.-i. Yamaki, *J. Electrochem. Soc.* **2011**, *158*, A1067.
[23] J. Kang, S. Baek, V. Mathew, J. Gim, J. Song, H. Park, E. Chae, A. K. Rai, J. Kim, *J. Mater. Chem.* **2012**, *22*, 20857.
[24] K. Saravanan, C. W. Mason, A. Rudola, K. H. Wong, P. Balaya, *Adv. Energy Mater.* **2013**, *3*, 444.
[25] Z. L. Jian, C. C. Yuan, W. Z. Han, X. Lu, L. Gu, X. K. Xi, Y. S. Hu, H. Li, W. Chen, D. F. Chen, Y. C. Ikuhara, L. Q. Chen, *Adv. Funct. Mater.* **2014**, *24*, 4265.
[26] B. L. Cushing, J. B. Goodenough, *J. Solid State Chem.* **2001**, *162*, 176.
[27] K. Du, H. W. Guo, G. R. Hu, Z. D. Peng, Y. B. Cao, *J. Power Sources* **2013**, *223*, 284.
[28] W. X. Song, X. B. Ji, C. C. Pan, Y. R. Zhu, Q. Y. Chen, C. E. Banks, *Phys. Chem. Chem. Phys.* **2013**, *15*, 14357.
[29] H. G. Zhang, X. D. Yu, P. V. Braun, *Nat. Nanotechnol.* **2011**, *6*, 277.
[30] S. Arico, P. Bruce, B. Scrosati, J. M. Tarascon, W. Schalkwijk, *Nat. Mater.* **2005**, *4*, 366.

[31] P. G. Bruce, B. Scrosati, J. M. Tarascon, *Angew. Chem. Int. Ed.* **2008**, *47*, 2930.
[32] S. Chen, Y. L. Xin, Y. Y. Zhou, Y. R. Ma, H. H. Zhou, L. M. Qi, *Energy Environ. Sci.* **2014**, *7*, 1924.
[33] Q. Y. An, Q. L. Wei, L. Q. Mai, J. Y. Fei, X. Xu, Y. L. Zhao, M. Y. Yan, P. F. Zhang, S. Z. Huang, *Phys. Chem. Chem. Phys.* **2013**, *15*, 16828.
[34] Y. G. Guo, J. S. Hu, L. J. Wan, *Adv. Mater.* **2008**, *20*, 2878.
[35] A. Q. Pan, H. B. Wu, L. Yu, T. Zhu, X. W. Lou, *ACS Appl. Mater. Interfaces* **2012**, *4*, 3874.
[36] H. Liu, Y. Wang, H. Li, W. Yang, H. Zhou, *ChemPhysChem* **2010**, *11*, 3273.
[37] C. B. Zhu, K. P. Song, P. A. Aken, J. Maier, Y. Yu, *Nano Lett.* **2014**, *14*, 2175.
[38] K. Saravanan, C. W. Mason, A. Rudola, K. H. Wong, P. Balaya, *Adv. Energy Mater.* **2013**, *3*, 444.
[39] W. C. Duan, Z. Q. Zhu, H. Li, Z. Hu, K. Zhang, F. Y. Cheng, J. Chen, *J. Mater. Chem. A* **2014**, *2*, 8668.
[40] D. Duffy, M. Barrett, B. Glennon, *Cryst. Growth Des.* **2013**, *13*, 3321.
[41] H. Qin, M. X. Zha, Z. Y. Ma, F. Q. Zhao, S. Y. Xu, H. X. Xu, *Propellants Explos. Pyrotech.* **2014**, *39*, 694.
[42] Z. L. Jian, W. Z. Han, X. Lu, H. X. Yang, Y. S. Hu, Jing Zhou, Z. B. Zhou, J. Q. Li, W. Chen, D. F. Chen, L. Q. Chen, *Adv. Energy Mater.* **2013**, *3*, 156.
[43] X. L. Wu, L. Y. Jiang, F. F. Cao, Y. G. Guo, L. J. Wan, *Adv. Mater.* **2009**, *21*, 2710.
[44] Y. Z. Li, Z. Zhou, X. P. Gao, J. Yan, *J. Power Sources* **2006**, *160*, 633.
[45] J. C. Zheng, X. H. Li, Z. X. Wang, H. J. Guo, Q. Y. Hu, W. J. Peng, *J. Power Sources* **2009**, *189*, 476.
[46] M. V. Reddy, G. V. S. Rao, B. V. R. Chowdari, *J. Power Sources* **2010**, *195*, 5768.
[47] M. M. Ren, Z. Zhou, Y. Z. Li, X. P. Gao, J. Yan, *J. Power Sources* **2006**, *162*, 1357.
[48] M. Endo, C. Kim, K. Nishimura, T. Fujino, K. Miyashita, *Carbon* **2000**, *38*, 183.
[49] Z. L. Jian, L. Zhao, H. L. Pan, Y. S. Hu, H. Li, W. Chen, L. Q. Chen, *Electrochem. Commun.* **2012**, *14*, 86.
[50] H. Y. Wang, K. L. Huang, Y. Ren, X. B. Huang, S. Q. Liu, W. J. Wang, *J. Power Sources* **2011**, *196*, 9786.
[51] H. Y. Wang, W. J. Wang, Y. Ren, K. L. Huang, S. Q. Liu, *J. Power Sources* **2012**, *199*, 263.